A

DISTANCE MEASURES

For the sake of simplicity, only the distance between discrete 3D-surfaces represented by triangular meshes will be defined. A discrete 3D-surface is usually represented by a set of point $S = \{p^1, p^2, ..., p^n\}$ in $\mathbb{R}^3$ (vertices), and by a set $\mathcal{T}$ of triangles describing how the vertices from S are linked together. Thus, the similarity between two surfaces is measured by computing distances between the respective points sets. Let define a point p belonging to the surface S, and the point q belonging to the surface S'.

Euclidean distance between two points

The Euclidian distance is defined as the shortest possible path through space between two points (also named the $L^2 - norm$) and is defined as:

$$D(p,q) = \|p - q\|_2 = \left(\sum_{n=0}^{3} |p_i - q_i|^2\right)^{\frac{1}{2}} \tag{A.1}$$

Node to surface distance

The distance $D^s(p, S')$ from the point p to the surface S' is defined as

$$D^s(p, S') = min_{q \in S'} \|p - q\|_2 \tag{A.2}$$

Minimal distance between two surfaces

The minimal distance between two surfaces S and S' is defined as

$$D^S_{min}(S, S') = min_{p \in S}\{D^s(p, S')\} \tag{A.3}$$

Maximal distance between two surfaces

The maximal distance between two surfaces S and S' is defined as

$$D^S_{max}(S, S') = max_{p \in S}\{D^s(p, S')\} \tag{A.4}$$

Mean distance between two surfaces

The mean distance between two surfaces S and S' is defined as

$$D^S_{mean}(S, S') = \frac{1}{|S|} \sum_{p \in S} D^s(p, S') \tag{A.5}$$

where $|S|$ is the number of nodes belonging to the surface S.

Hausdorff distance between two surfaces

The Hausdorff distance [75] between two surfaces is defined as

$$H(S, S') = max\{D^S_{max}(S, S'), D^S_{max}(S', S)\} \tag{A.6}$$

Modified Hausdorff distance between two surfaces

The modified Hausdorff distance between two surfaces is defined as

$$H(S, S') = max\{D^S_{mean}(S, S'), D^S_{mean}(S', S)\} \tag{A.7}$$

Dubuisson and Jain [36] have studied 24 measures to assess the similarities between two discrete surface meshes. According to the authors, the Hausdorff distance has the best performance for object matching.

B

Mesh Convergence

In finite element modeling, a finer mesh usually results in a more accurate solution. However, as a mesh is made finer, the computation time increases. To get a mesh that satisfactorily balances accuracy and computing resources, a mesh convergence study has to be performed.

In this scope, the breast and muscle geometries were meshed with different mesh sizes; the minimal elements sizes was set to $7mm$ and the maximal element size was varied between $\{7mm, 10mm, 13mm, 15mm, 17mm, 20mm\}$. The compression paddles geometries were meshed with a constant element size of $1mm$. The number of elements obtained for each mesh size is given in Table B.1. For the mesh size equal to 17 mm, a higher number of elements was obtained when compared to the mesh size of 15mm. This was due to the fact that the mesh size is defined by the maximal and minimal elements size, a higher number of *small* elements was needed to cover the areas smaller than the *large* elements. In such meshes, the elements density is normally concentrated on the geometry's corners or narrow spaces which, in our case, does not coincide with the region of interest.

Mesh size	20mm	17mm	15mm	13mm	10mm	7mm
Nb. of elements	8367	10897	8099	10751	18453	65785

Table B.1: Number of elements obtained for each mesh size.

As the model was conceived to compute breast deformation under compression, an equivalent simulation was performed to estimate the optimal mesh size. Starting from the breast supine geometry, the gravity was applied in the posterio-anterior direction. Then, the right breast was compressed between the paddles (Figure B.1). The strain distribution over the breast volume as well as the compression force for each mesh size are given in Figure B.1.

One can see that the force intensity converges from a mesh size equal to $15mm$, however the strain distribution over the breast volume has still a poor estimation when compared to the strain distribution obtained with a mesh size equal to 7mm. The visual analysis of

[indiquer que le hardware utilisé ne l'a pas permis de réaliser des simulations avec des éléments de 5mm.]

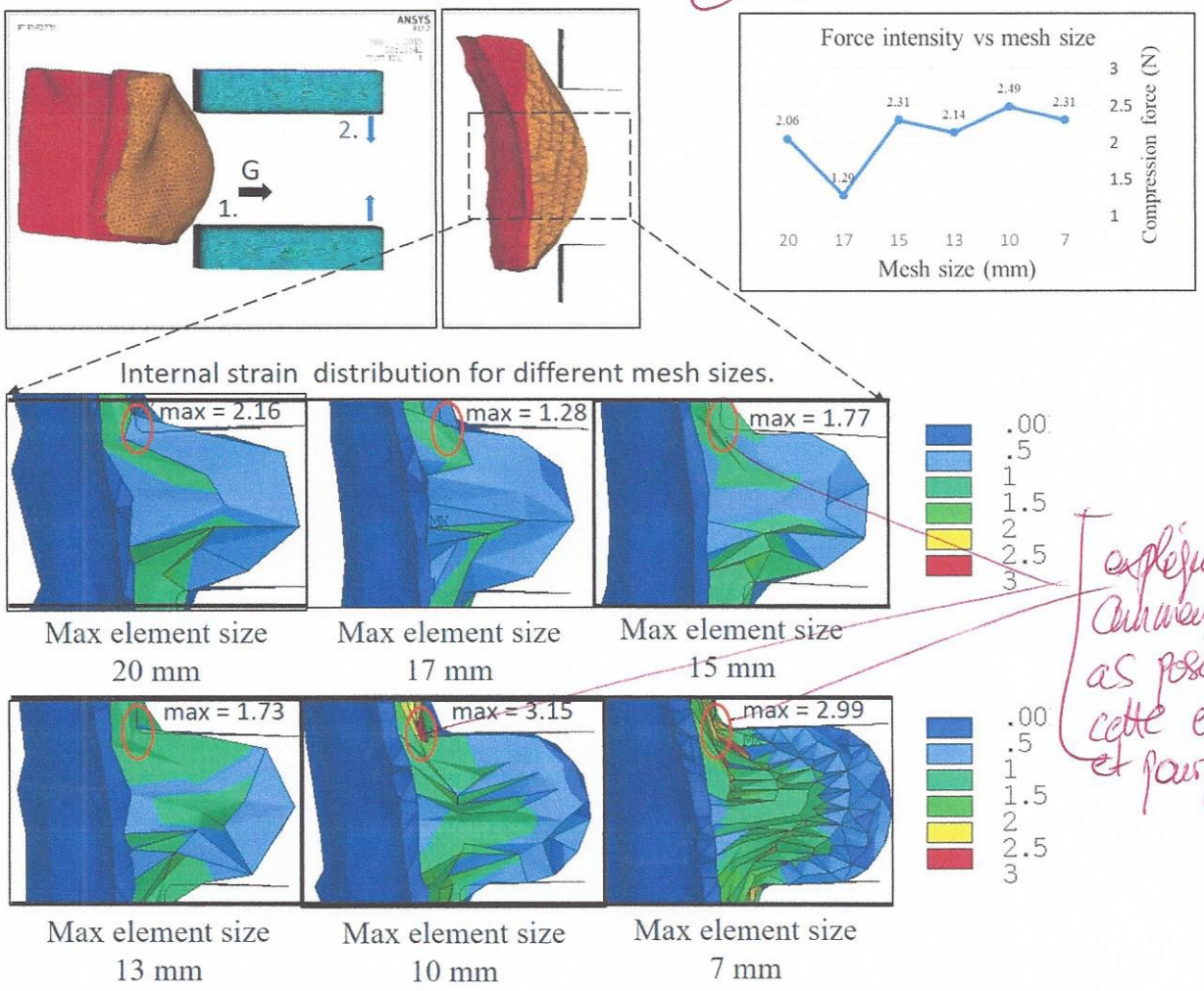

[expliquer comment tu as procédé cette ellipse et pourquoi]

Figure B.1: Internal strain distribution in function of the elements size.

the strain distribution and amount of penetration at the surface contact show that starting from a mesh size equal to 10mm, the results are estimated well enough .

[Comment est-ce que tu le définis ? → indiquer que tu te bases sur l'analyse de la force vs mesh size et que les images sont juste illustratives]

[Ah bon!? Mon sentiment est que, visuellement, il faut 7mm au moins... expliquer plus]

[pénétration de quoi ? à expliquer ici]

[expliquer pourquoi la force de compression plutôt que le stress]

C

Bondary conditions
contact models

The proposed biomechanical model consists of two bodies, one representing the pectoral cage with the pectoral muscle, and the second representing the breast soft tissue. Between the two bodies, a contact surface is defined in order to model tissues mechanics at the juncture interface.

The next section describes the implementation of different interaction models tested during the model development process. Since the breast tissues are always attached to the pectoral muscle (Figure C.1), the contact surface was modeled using *bonded* and *no-separation frictional* interaction models only.

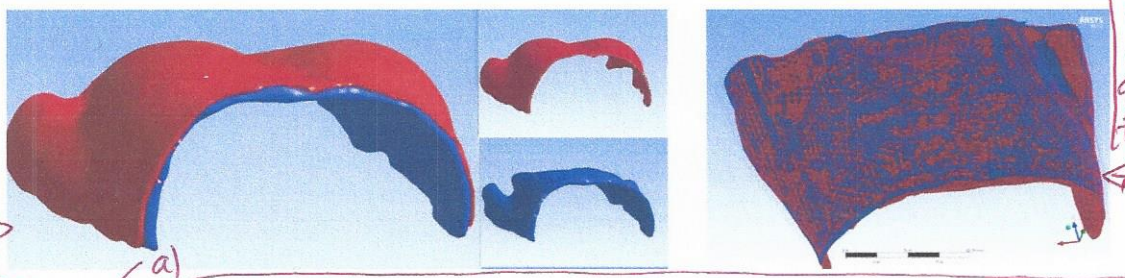

Figure C.1: The two bodies representing the thoracic cage and breast with the associated contact surface. Blue surface, the target surface, red surface - contact surface.

The results for pure bonded and pure no-separation sliding models, as well as one combined contact surface, are listed bellow. For some contacts models, because of large instabilities or a poor fidelity to the real breast mechanics, only partial results are presented.

Bonded contact surface

First, a pure bounded contact was used to model the interaction between the breast and the pectoral muscle. To achieve realistic breast deformation, extremely low values of equivalent

Young's modulus and Poisson ratio were needed ($\lambda_{breast} = 0.3kPa$ and $\nu_{breast} = 0.45$). An example of breast deformation in prone and supine configuration is illustrated in Figure C.2.

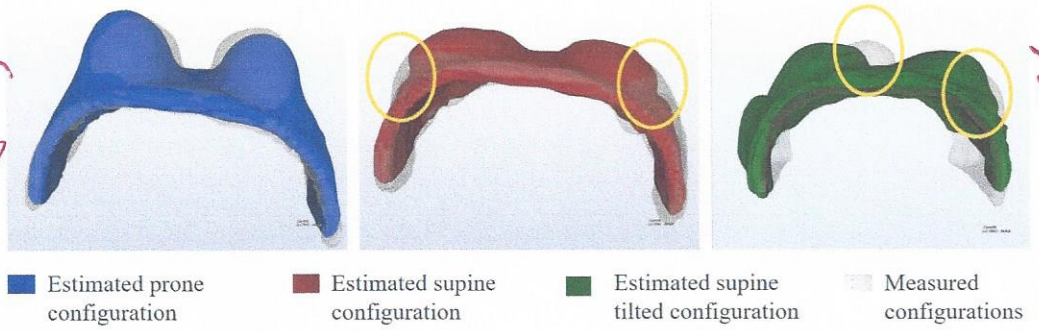

Figure C.2: Resulting breast deformation with a bonded contact model.

One can see that, even if the breast geometry in prone position is well estimated, the ones in supine and supine tilted configurations are constrained laterally. Moreover, a important volume variation was observed which is not a characteristic of breast changes under gravity loading. The volume variation is due to a too low value of the Poisson ratio.

Sliding contact surface

Pure sliding contact surface was considered in order to allow larger tissues displacements on lateral direction. The breast sliding over the muscle surface was modeled using the Coulomb friction low (Section 2.3.2). Additional boundary condition were set by imposing zero-displacement on the right, left, superior and inferior mesh boundaries representing the breast volume (see Figure 3.11 for a recall on different mesh boundaries). This model caused large convergence problems because of breast tissues over-sliding. It was obvious that the model needs more boundary conditions in order to ~~archive~~ convergence. Moreover, a non-linear and a non-uniform sliding model was needed in order imitate the behavior of rich fibrous areas where the breast is attached to the chest wall (see Section 1.1.3 for a recall on breast anatomy).

Mixt contact surface

In order to limit breast tissues sliding, a mixt contact surface was defined. Herein, the contact surface consists of two complementary areas (Figure C.3), one modeled as bonded contact and the second one modeled as no-separation sliding contact. The regions corresponding to the bounded contact are defined following the anatomical structures ~~were~~ the concentration of fibrous tissues is significantly higher. Such regions are encountered along the muscle surface where the superficial muscle fascia meets the breast suspensory ligaments ~~as~~ the inframammary ligament, the deep medial ligament or the deep lateral ligament.

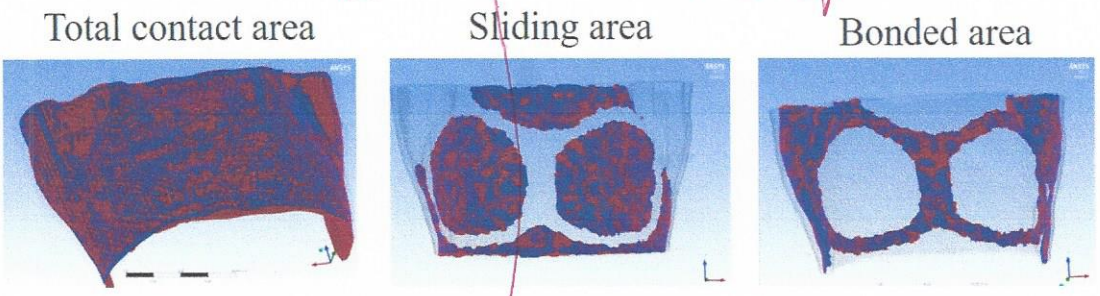

Figure C.3: The contact surface divided in two regions: sliding region and bonded region.

Using such a contact model improves substantially the estimate of the supine breast configuration. However, because of a high deformation gradient imposed at the juncture border between the two contact areas, solution convergence problems were met. Moreover, when the supine configuration is estimated, several folds are created at the skin surface (Figure C.4). The same types of folds were obtained in supine tilted configuration creating large convergence problems because of tissues superposition.

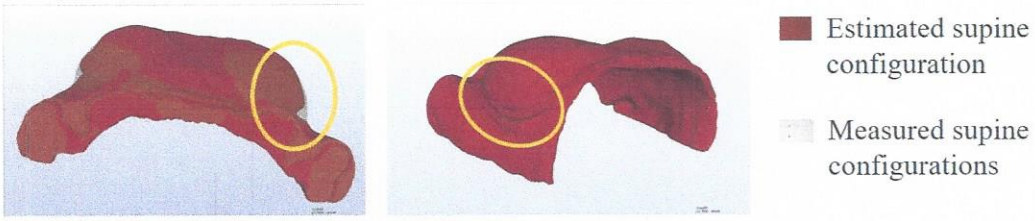

Figure C.4: The contact surface divided in two regions: sliding region and bonded region.

This last described model has provided satisfactory results, however it implies important solution convergence problems. Therefore, the model was improved by replacing the bonded contact regions with stiff ligaments connecting the breast tissues to the muscle. Contrary to the bonded contact, the ligaments preclude progressively the breast tissues from sliding and allow a slight displacement avoiding the creation of folds. Moreover, an additional layer modeling the deep layer of breast superficial fascia was added at the juncture surface between breast and muscle. Knowing that the fascia is stiffer than the breast soft tissues, it controls the amount of sliding and facilitates the solution convergence. For more information on ligaments and fascia mechanical properties, see Section 3.4.